JOURNAL OF COMPUTATIONAL PHYSICS 81, 193–205 (1989)

SARLAC: A Relativistic Electron Beam Code

GLENN JOYCE, RICHARD HUBBARD, MARTIN LAMPE, AND STEVEN SLINKER

Plasma Physics Division, Naval Research Laboratory, Washington, DC 20375-5000

Received October 24, 1987; revised April 12, 1988

SARLAC is a particle simulation code for studying the propagation of ultra-relativistic electron beams. It is used to study the nonlinear evolution of the resistive hose instability. We have developed a fast, semi-implicit, iterative field solver which allows us to include a large number of Fourier modes in the azimuthal direction. The solver iterates about a solution of the field equations dominated by the axisymmetric ($m=0$) conductivity. This technique has proved to be quite successful. We compare some results of the code with those obtained from a linearized hose simulation code and show differences when the hose oscillations reach large amplitude. © 1989 Academic Press, Inc.

We have recently written a number of simulation codes to test various aspects of the resistive hose instability in high energy electron beams propagating in resistive plasmas. Most methods used previously for treating the instability were restricted to small instability amplitudes. These are considered to be of practical interest because large amplitude hose-like oscillations quickly destroy the integrity of the beam, and because, under appropriate circumstances, the instability "saturates" in the linear regime. That is to say, the hose instability is convective in the beam frame, and therefore, at any given point in the beam may reach a maximum which is still small followed by a decay of the instability as the disturbance convects past. Near term experiments, however, are frequently more unstable than can be treated by linear models, so we have developed a particle simulation code which can follow the evolution of an instability into the nonlinear regime [1–3]. Similar codes have been written by Godfrey [4] and Freeman [5].

The nonlinear code has borrowed heavily from two of our previous codes, SIMM0 [6] and SIMM1 [7] which are particle simulation codes for axisymmetric beams and beams with small amplitude hose motions. The particle dynamics of those two codes are followed in Cartesian coordinates so the SARLAC code differs from these primarily in the calculation of the electromagnetic fields. We have developed a fast iterative field solver which allows us to include a large number of Fourier modes in the azimuthal direction.

The code employs many of the approximations found in most linearized propagation models [8–10]. The variables z and t are replaced by z and $\zeta = ct - z$ (the distance from the beam head), and all particles remain at constant ζ since v_z is assumed to be the velocity of light. The frozen approximation is used in the field

0021-9991/89 $3.00

equations, and the same conductivity model used in the VIPER [8] code is employed. Beam dynamics are treated using standard particle simulation techniques. Current densities, fields, and conductivity are calculated on a polar grid (u, Θ, ζ) with $u = \sqrt{r}$ as the radial variable. The lay-down scheme for the particles is quadratic in the radial and azimuthal variables and nearest grid point in the axial variable.

The ultra-relativistic approximations used in SARLAC lead to a code structure which is substantially different from "conventional" particle simulations. Information can only flow in one direction: toward larger ζ. Also, since individual particles always remain at the same axial position within the beam, the simulation can treat one slice at a time, thus reducing the number of particles in the simulation at any time to $\sim 10^4$. Each beam slice is propagated forward in z until the maximum propagation range, $z_{\max}$ is reached. At this point, particles are loaded into the next slice, and the process is repeated. The current density J, conductivity σ, and potentials $\mathcal{A}$ and ϕ from the previous slice must be read from the disk. The axial step $\Delta\zeta$ is variable, and the code has the option of subgridding the field and conductivity integrations on a finer axial mesh than is used for the particles. All diagnostics are done with post-processors. The dimensionless units used in VIPER and SIMM1 are employed throughout [7, 8].

Electromagnetic Fields

The frozen approximation to Maxwell's equations is performed in a gauge suggested by Lee [11]. The equations are

$$\nabla_\perp^2(\mathcal{A} + \phi) - \frac{\partial^2 \mathcal{A}}{\partial \zeta^2} = -J_b + \sigma \frac{\partial \mathcal{A}}{\partial \zeta} \tag{1}$$

$$-\nabla_\perp^2 \frac{\partial \mathcal{A}}{\partial \zeta} = -\nabla_\perp \cdot (\sigma \nabla_\perp \phi), \tag{2}$$

with the frozen condition

$$\frac{\partial}{\partial \zeta} \mathbf{A}_\perp = \frac{\partial \mathcal{A}}{\partial z} = \frac{\partial \phi}{\partial z} = \frac{\partial \mathbf{A}_\perp}{\partial z} = 0 \tag{3}$$

and $\mathcal{A} = A_z - \phi$.

The boundary conditions for $\mathcal{A}$ and ϕ are

$$\begin{aligned} \mathcal{A}(r) &= 0, \qquad \zeta = 0 \\ \phi(r) &= 0, \qquad \zeta = 0 \\ \mathcal{A}(\zeta) &= 0, \qquad r = R_{\max} \\ \phi(\zeta) &= 0, \qquad r = R_{\max}. \end{aligned}$$

These conditions correspond to a beam propagating at the speed of light in a perfect conductor of radius $R_{\max}$.

Equations (1) and (2) are "diffusion-like" equations with the resistivity acting as a diffusion coefficient. There is, then, a preferred direction of information flow in ζ which is always toward larger ζ. This is consistent with the ultrarelativistic condition. The conditions of Eqs. (3) are valid as long as the particle motions are paraxial. This approximation breaks down in the limit of extremely large hose motions. In practice, because the code is written in a cylindrical coordinate system with a limited number of azimuthal modes, the code becomes invalid long before the paraxial approximation becomes invalid.

For completeness, we write the fields and particle dynamics as

$$\begin{aligned} E_z &= -\frac{\partial \mathcal{A}}{\partial \zeta} \\ \mathbf{E}_\perp &= -\nabla_\perp \phi \\ \frac{\partial(\gamma m \mathbf{v}_\perp)}{\partial z} &= +q/c \nabla_\perp \mathcal{A} \\ \frac{\partial \gamma}{\partial z} &= \frac{qE_z}{mc^2}. \end{aligned} \tag{4}$$

The equations are similar in form to the EMPULSE [12] equations with an additional term $\partial^2 \mathcal{A}/\partial \zeta^2$ in the first equation. A fully implicit method for solving these equations has been developed by Hui [13]. That field solver Fourier analyzes the azimuthal dependence of all quantities into a series of modes $\exp(im\Theta)$ and performs a full complex matrix inversion, which is extremely time consuming and thus impractical for long simulation studies. The major advance of the SARLAC code is the development of a field solver which does not require a complete matrix inversion. The SARLAC field solver uses a predictor-corrector method which iterates about a solution obtained by assuming that the axisymmetric ($m=0$) conductivity dominates the solution. The $m=0$ mode of any positive definite function is always larger than any other single mode and in the case of beam generated conductivity which is generated all along the beam axis, this mode is large compared to the other modes even for large excursions of the beam from axisymmetry, as long as the front of the beam is on the axis.

In the Appendix, we develop an algorithm for numerically solving Eq. (1) over the interval $\zeta_n \leqslant \zeta \leqslant \zeta_{n+1}$. The solution is

$$\begin{aligned} \mathcal{A}^{n+1} = \Big\{ & \mathcal{A}^n - \mathcal{A}^{n-1} \frac{1}{2\sigma \Delta\zeta}(1 - e^{-\sigma \Delta\zeta}) + J_b \frac{1}{\sigma^2}(\sigma \Delta\zeta - (1 - e^{-\sigma \Delta\zeta})) \\ & + \nabla_\perp^2 (\mathcal{A} + \phi) \frac{1}{\sigma^2}(\sigma \Delta\zeta - (1 - e^{-\sigma \Delta\zeta})) \Big\} \Big/ \left(1 - \frac{1}{2\sigma \Delta\zeta}\left(1 - e^{-\sigma \Delta\zeta}\right)\right), \end{aligned} \tag{5}$$

where the superscript n represents the function evaluated at ζ_n. The conductivity, σ, is evaluated in the interval (ζ_n, ζ_{n+1}). Rewrite Eq. (5) as

$$\mathcal{A}^{n+1} = F(\mathcal{A}^n, \mathcal{A}^{n-1}; J_b, \sigma) + \nabla_\perp^2(\mathcal{A} + \phi) f(\sigma), \tag{6}$$

where

$$F(\mathcal{A}^n, \mathcal{A}^{n-1}; J_b, \sigma) = \left\{ \mathcal{A}^n - \mathcal{A}^{n-1} \frac{1}{2\sigma \Delta\zeta}(1 - e^{-\sigma\Delta\zeta}) + J_b \frac{1}{\sigma^2}(\sigma\Delta\zeta - (1 - e^{-\sigma\Delta\zeta})) \right\} \Big/ \left(1 - \frac{1}{2\sigma\Delta\zeta}(1 - e^{-\sigma\Delta\zeta})\right) \tag{7}$$

and

$$f(\sigma) = \frac{(\sigma\Delta\zeta - (1 - e^{-\sigma\Delta\zeta}))/\sigma^2}{(1 - 1/2\sigma\Delta\zeta(1 - e^{-\sigma\Delta\zeta}))}. \tag{8}$$

We see that

$$f(\sigma) \to \Delta\zeta/\sigma \qquad \text{for} \quad \sigma \text{ large}$$
$$f(\sigma) \to (\Delta\zeta)^2 \qquad \text{for} \quad \sigma \text{ small.}$$

Equation (2) is simply differenced to give

$$-\nabla_\perp^2 \frac{\mathcal{A}^{n+1} - \mathcal{A}^n}{\Delta\zeta} = -\nabla_\perp \cdot (\sigma \nabla_\perp \phi). \tag{9}$$

Note that we have omitted the superscripts from some of the $\mathcal{A}$ and ϕ terms in Eqs. (6) and (9). By choosing these terms at the nth or $(n+1)$th (or some combination of these levels), the differencing can be made explicit or implicit to some formal accuracy. Our experience has been that the algorithms for these equations are numerically unstable if they are explicitly differenced. An implicit differencing can eliminate the instability, but at the expense of a complicated matrix inversion due to the azimuthal coupling of σ with the potentials. To avoid this, we have chosen instead to rewrite Eqs. (6) and (9) as

$$\mathcal{A}^{n+1} - \nabla_\perp^2(\mathcal{A} + \phi) f_0(\phi) = F(\mathcal{A}^n, \mathcal{A}^{n-1}; J_b, \phi) + \nabla_\perp^2(\mathcal{A} + \phi)(f(\phi) - f_0(\phi)) \tag{10}$$

and

$$-\nabla_\perp^2 \frac{\mathcal{A}^{n+1} - \mathcal{A}^n}{\Delta\zeta} + \nabla_\perp \cdot (\sigma_0 \nabla\phi) = -\nabla_\perp \cdot (\sigma - \sigma_0)\nabla_\perp \phi, \tag{11}$$

where

$$f_0(\sigma) = \frac{1}{2\pi}\int_0^{2\pi} f(\sigma(\theta))\, d\theta, \qquad \sigma_0 = \frac{1}{2\pi}\int_0^{2\pi} \sigma(\theta)\, d\theta. \tag{12}$$

Equations (10) and (12) are formally the same as Eqs. (6) and (9). However,

since σ_0 does not vary in azimuth, the left-hand sides of these equations can be evaluated at the upper level without involving convolution sums, which leads to a tridiagonal form for $\mathcal{A}^{n+1}$ and ϕ^{n+1}. The right-hand sides can be evaluated explicitly since the functions are known. The simplest differencing scheme leads to a first-order algorithm. We have chosen a predictor-corrector method which is accurate to second order and is quite stable. For the sake of brevity, we will not go into the details of the differencing, but they are easily reproduced. We solve the equations in the Fourier transformed space (u, m, ζ) always keeping the right-hand sides explicit. The right-hand sides, then, can be evaluated in (u, Θ, ζ) thus avoiding convolution sums on the right-hand sides as well. The method of adding and subtracting averaged terms to gain stability without full matrix inversions is similar to that used by Harned [14] for a different set of equations.

Numerical Issues

In SARLAC, the number of modes N_Θ and radial mesh size Δu remain fixed throughout a run. Typically, $N_\Theta = 16$ or 32, and $\Delta u = 0.125\, a_0^{1/2}$, where a_0 is a characteristic initial beam radius. The axial grid spacing $\Delta\zeta$ is specified for each slice at the beginning of the run. In general, $\Delta\zeta$ is allowed to increase with ζ, since (at least in the linear regime) the ζ-variation is characterized by the dipole decay length, $\pi\sigma(r=0)a_0^2/2c$, which usually increases monotonically throughout the pulse. However, field solver tests have shown that the axial step size must often be reduced when the beam displacement is large. This is accomplished by subgridding the field and conductivity integrations. In most cases, $\Delta\zeta$ is chosen to be small enough that subgridding is rarely involved.

The beam current density J_b is intrinsically noisy because of the statistical fluctuations arising from the small number of particles in each $u-\Theta$ grid cell. This is particularly troublesome near $u=0$. Increasing the number of simulation particles per slice reduces noise problems but is computationally expensive. Other methods which we have employed include accumulating current densities on a coarser radial mesh than is used for the field solver and interpolating, averaging over the first few radial grid points and using an azimuthal filtering technique near the origin.

Originally, we assigned random initial values of Θ to the particles but found that this procedure resulted in large initial noise levels for the hose instability and in substantial drifts in the beam head. The noise effects are reduced by loading the particles in pairs on opposite sides of the beam. If the velocities are also loaded symmetrically, the $m=1$ azimuthal mode is eliminated in the initial stages of propagation. A small specified perturbation can be added to all particles in a given beam slice to start the hose instability in a controlled manner. Higher order Fourier modes can be suppressed by loading four or more particles with the appropriate symmetry. The elimination of higher order modes has not proven particularly useful since the nonlinear coupling of these modes is usually too weak to introduce significant hose growth.

The scattering of beam electrons by the neutral gas is known to play an important role in the evolution of the beam. SARLAC uses an algorithm originally developed by Chambers [6, 15] and modified by Hughes and Godfrey [16] to provide a more accurate representation of the scattering process. Each beam particle is periodically scattered through a randomly chosen angle whose characteristic magnitude is determined by the energy and the gas density. After an initial transient phase, the beam reaches a quasi-static equilibrium. The beam radius then expands slowly due to scattering. If beam particles are loaded in pairs, a straightforward application of the scattering algorithm will eventually introduce significant noise and drifts at the beam head. These effects can be eliminated by scattering the particles in pairs. The random velocity $\Delta \mathbf{v}_i$ applied to a given particle at a given z step is balanced by adding $-\Delta \mathbf{v}_i$ to the particle with which it was originally paired. This technique has been highly successful in practice.

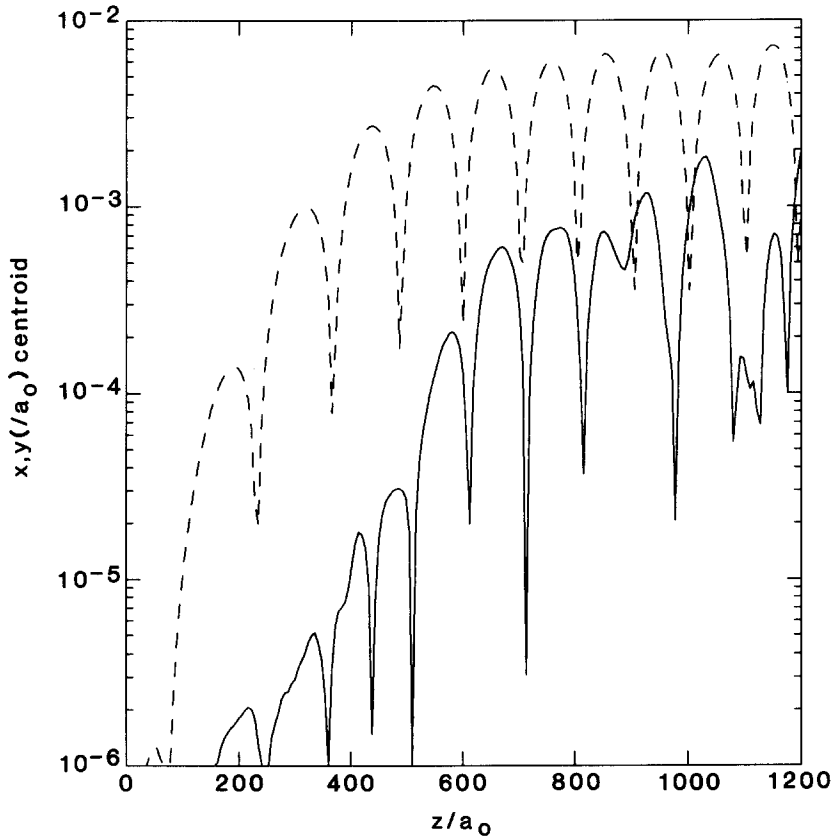

FIG. 1. Plot of the beam x and y centroids at $\zeta = 50$ cm as a function of the beam propagation distance. The initial perturbation $y_0 = 10^{-5}$ so that saturation is reached while the hose instability is in the linear regime. The dashed line is the y centroid and the solid line is the x centroid. The initial perturbation is chosen in the y direction.

The simulation code is best suited for treating cases in which the hose displacement is a few times the nominal radius a_0. The coordinate system is chosen to have the finest resolution in both the radial and azimuthal directions near the origin. For extremely large beam oscillations, when the beam displacement reaches a substantial fraction of the wall radius, the accuracy of the simulation is reduced and the field solver is sometimes subject to numerical instabilities. The field solver instabilities appear to be triggered by conditions in which the local conductivity centroid gets far enough off the coordinate system axis that the conductivity is not dominated by the $m=0$ mode. Usually this conductivity is generated by avalanche due to strong, localized, electric fields; such fields can arise when the hose motion is quite nonlinear [1]. Evidence for very strong electric fields associated with nonlinear hose motion has been seen in the ETA experiments [17], so the strong fields may be physical (up to a point). Considerable effort has been made to make the field solver more robust, and with careful differencing we have had some success.

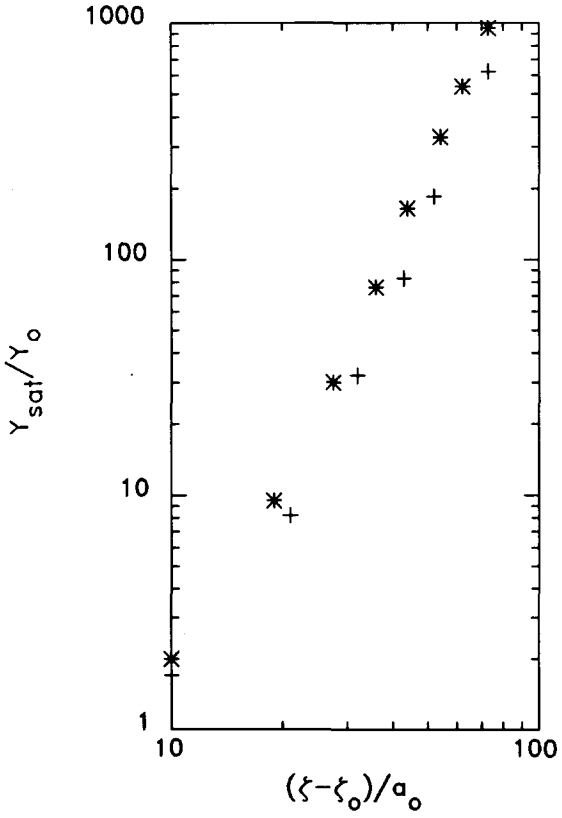

FIG. 2. Plot of the saturated hose amplitude as a function of the distance back from the point of the initial perturbation. The SARLAC results are marked with *'s while the VIPER results are marked with +'s.

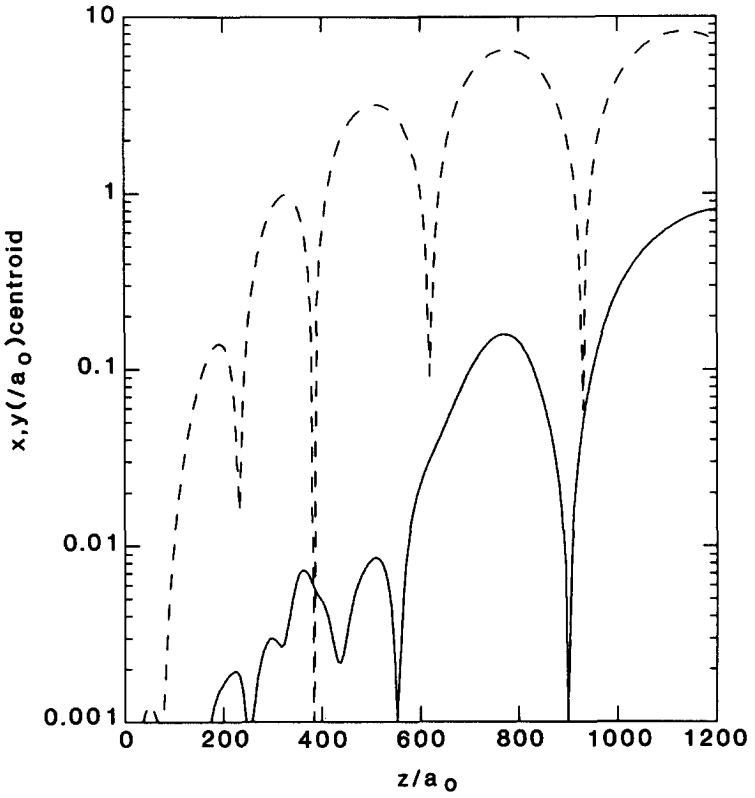

FIG. 3. Plot of the beam x and y centroids at $\zeta = 50$ cm as a function of the beam propagation distance. The initial perturbation is $y_0 = 10^{-2}$ so that the hose instability becomes nonlinear. When the hose motion becomes large, the beam radius increases and the frequency of the oscillation decreases. Again, the dashed line is the y centroid and the solid line is the x centroid.

We have also found that these problems can be mitigated by using small ζ grids in regions where there are large hose amplitudes. Even so, we believe the code to be best suited for moderate hose oscillations.

NUMERICAL RESULTS

We have run the code under a variety of conditions. Many of the runs have been checked against the results of Hui and Lampe [13] and the agreement between these codes is satisfactory. We show here the results of two runs; one for small perturbations, in which the hose stays in the linear regime, saturates and decays, and one with moderate initial perturbations, for which the hose grows and becomes nonlinear. The parameters for both sets of runs are

$a_0 = 0.5$ cm, the beam radius.

$I = 10$ kA, the beam current .

$\gamma = 100$, the beam energy.

$\zeta_r = 15$ cm, the beam current rise length.

$a_w = 81a_0$, the outer radius of the simulation.

$y_{\text{pert}} = y_0 \sin 2\pi((\zeta - \zeta_0)/\zeta_0)$, the initial perturbation over the range

$$\zeta_0 < \zeta < 1.5\zeta_0, \qquad \zeta_0 = 10 \text{ cm}.$$

(Note, this perturbation is in the y direction.)

For the first run we used a very small initial hose amplitude $y_0 = 10^{-5}a_0$ which

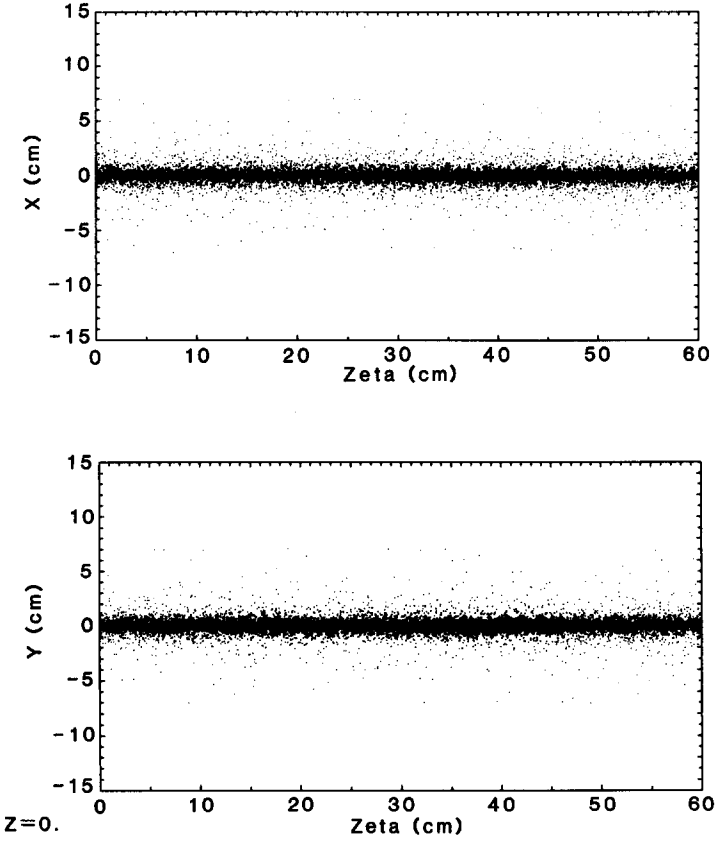

FIG. 4. Plot of the beam particle positions at $z = 0$. The particles are loaded with a Bennett distribution. The beam current increases with increasing ζ but this is not indicated by increasing numbers of particles because the particles are weighted with the charge.

kept the hose oscillations linear over the length of the beam. For this case, the hose instability grows and saturates as seen in Fig. 1. Figure 2 shows a comparison of the saturation amplitude at various distances from the beam head with the results of the linearized VIPER code, which uses the multi-component model [18] to represent the particle dynamics approximately. The oscillation frequency, growth rate, and saturation amplitude agree quite well with the VIPER code [8].

The parameters chosen for the second run were the same except for a much larger initial amplitude $y_0 = 10^{-2} a_0$, so that the hose oscillations would become nonlinear. Figure 3 shows the growth of the hose through the x and y centroids of the beam. The dashed line is the y centroid which is much larger than x because the pertubation is initialized in y. After the hose displacements reach the order of the beam radius, the frequency of the oscillation decreases. This is because the beam is spreading in radius and the wavelength of the oscillation scales as the radius.

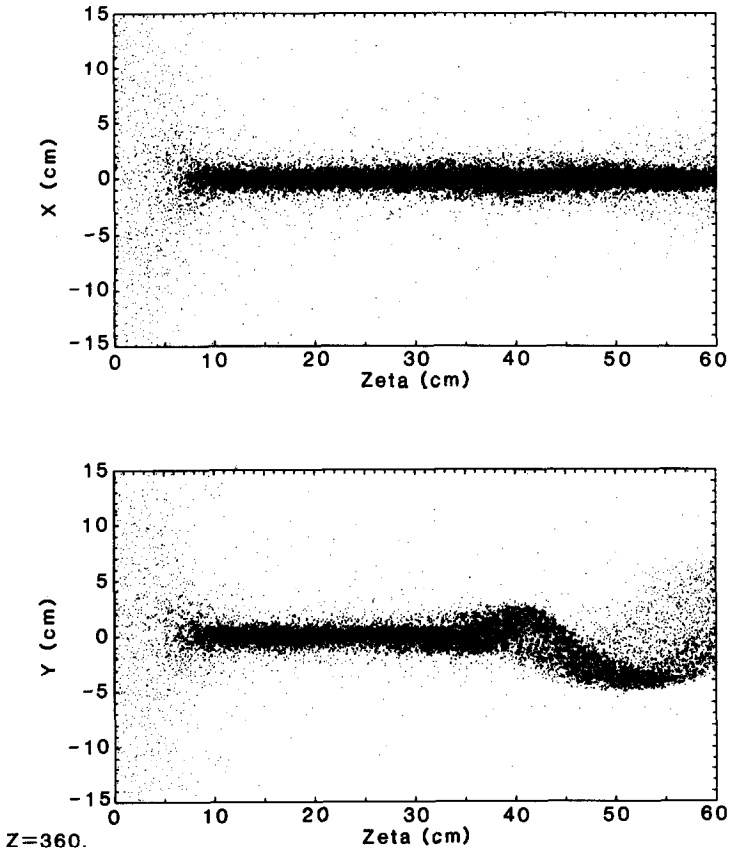

FIG. 5. Plot of the beam particle positions at $z = 360$ cm. The beam head has begun to blow off and the hose perturbation has grown enough to be easily seen.

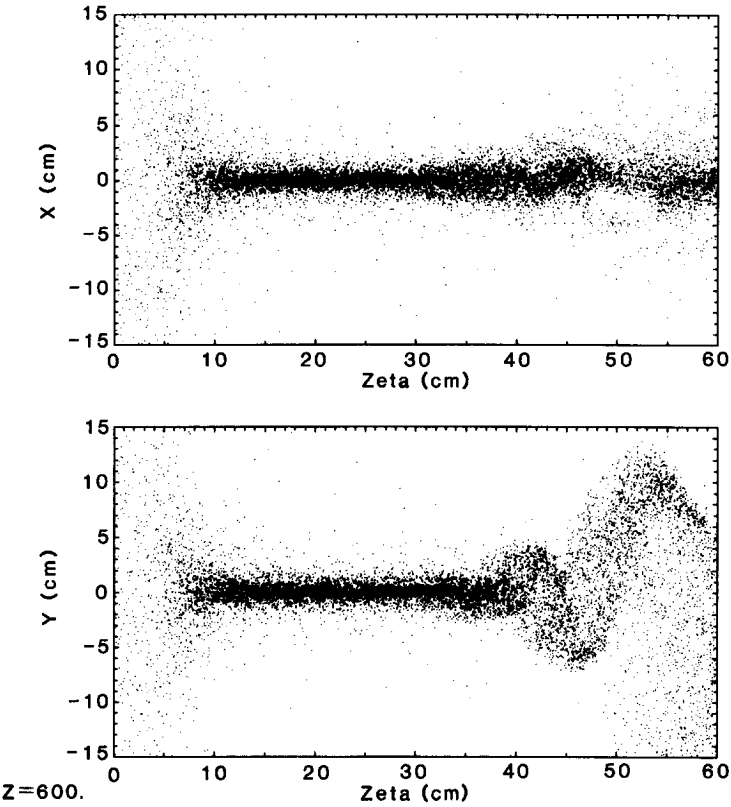

FIG. 6. Plot of the beam particle positions at $z = 600$ cm. The hose perturbation has grown so large that the tail of the beam is completely disrupted.

Figures 4–6 are beam particle plots at various distances of propagation.[1] We can see the development of the hose instability and the loss of the beam pinch as the instability becomes large.

APPENDIX

We have developed an algorithm to solve Eq. (1). Since the conductivity, σ, may be either large or small we need an algorithm which can be used for arbitrary σ. We write Eq. (1) as

$$e^{-\int \sigma d\zeta'} \frac{\partial}{\partial \zeta} e^{\int \sigma d\zeta'} \frac{\partial \mathcal{A}}{\partial \zeta} = \nabla_\perp^2 (\mathcal{A} + \phi) + J_b \tag{A1}$$

[1] To optimize the visual density of the plots, a randomly selected subset of the beam particles are plotted, rather than the entire beam.

and integrate the equation over the inverval ζ_n to ζ, where $\zeta_n \leqslant \zeta \leqslant \zeta_{n+1}$,

$$e^{\int \sigma d\zeta''} \frac{\partial \mathcal{A}}{\partial \zeta'}\bigg|_{\zeta_n}^{\zeta} = \int_{\zeta_n}^{\zeta} e^{\int \sigma d\zeta''} (\nabla_\perp^2 (\mathcal{A} + \phi) + J_b)\, d\zeta'. \tag{A2}$$

In order to evaluate the right-hand side of Eq. (A2), we assume that $\nabla_\perp^2(\mathcal{A}+\phi)+J_b$ does not change much over the interval $\Delta\zeta$ so that it can be evaluated at some intermediate point and taken outside the integral. In addition, we assume that to a good approximation, we can write $\int \sigma\, d\zeta'' \simeq \sigma(\zeta - \zeta_n)$, where σ is also evaluated somewhere on the interval. In practice, we know σ only at he midpoint of the interval, so that is the value we use. Making these approximations, we obtain

$$\frac{\partial \mathcal{A}}{\partial \zeta} = \frac{\partial \mathcal{A}}{\partial \zeta}\bigg|_{\zeta_n} e^{-\sigma(\zeta-\zeta_n)} + \overline{(\nabla_\perp^2(\mathcal{A}+\phi)+J_b)} \frac{1}{\sigma}(1 - e^{-(\zeta-\zeta_n)\sigma}). \tag{A3}$$

We integrate the equation once again to obtain $\mathcal{A}^{n+1}$,

$$\begin{aligned} \mathcal{A}^{n+1} = \mathcal{A}^n - \frac{\partial \mathcal{A}}{\partial \zeta}\bigg|_{\zeta_n} \frac{1}{\sigma}\left[e^{-\sigma(\zeta-\zeta_n)}\right]_{\zeta_n}^{\zeta_{n+1}} \\ + \overline{(\nabla_\perp^2(\mathcal{A}+\phi)+J_b)} \frac{1}{\sigma}\left[\zeta + \frac{1}{\sigma} e^{-\sigma(\zeta-\zeta_n)}\right]_{\zeta_n}^{\zeta_{n+1}}. \end{aligned} \tag{A4}$$

We center the $\partial\mathcal{A}/\partial\zeta$ derivative at ζ_n and obtain

$$\begin{aligned} \mathcal{A}^{n+1} = \Big\{ \mathcal{A}^n - \mathcal{A}^{n-1} \frac{1}{2\sigma\,\Delta\zeta}(1 - e^{-\sigma\Delta\zeta}) \\ + \overline{(\nabla_\perp^2(\mathcal{A}+\phi)+J_b)} \frac{1}{\sigma^2}(\sigma\,\Delta\zeta - (1 - e^{-\sigma\Delta\zeta})) \Big\} \\ \div \left(1 - \frac{1}{2\sigma\,\Delta\zeta}(1 - e^{-\sigma\Delta\zeta})\right). \end{aligned} \tag{A5}$$

If the right-hand side of Eq. (A1) and σ are constant in ζ, this algorithm represents an exact solution to the differential equation. The accuracy of the algorithm is determined by the variability of the functions and not by the size of σ. This is an important property of the solution, since σ varies over several orders of magnitude from the head to tail of the beam, but generally does not change much over a grid interval.

ACKNOWLEDGMENTS

We would like to thank Drs. Bertram Hui and Richard Fernsler for their work on the code models and to Dr. Wahab Ali for his contributions to the conductivity model. We also want to acknowledge Drs. Keith Brueckner, Frank Chambers, William Fawley, Leon Feinstein, John Freeman, Brendan

Godfrey, William Sharp, and John Wagner, all of whom had an influence on the development of the code. This work was supported by the Defense Advanced Research Projects Agency under ARPA Order 4395, Amendement 63, and monitored by the Naval Surface Warface Center.

REFERENCES

1. R. F. FERNSLER, R. F. HUBBARD, B. HUI, G. JOYCE, M. LAMPE, AND Y. Y. LAU, *Phys. Fluids* **29**, 3056 (1986).
2. R. F. HUBBARD, G. JOYCE, S. P. SLINKER, M. LAMPE, AND J. M. PICONE, *Bull. Amer. Phys. Soc.* **30**, 1583 (1985).
3. R. F. HUBBARD, S. P. SLINKER, G. JOYCE, AND M. LAMPE, *Bull. Amer. Phys. Soc.* **31**, 1429 (1986).
4. B. B. GODFREY AND D. R. WELCH, "The IPROP Three-Dimensional Beam Propagation Code," in *Proceedings, 12th Conf. Numerical Simulation of Plasmas, San Francisco, 1987*, paper CM1.
5. J. R. FREEMAN, J. W. POUKEY, J. S. WAGNER, AND R. S. COATS, *J. Appl. Phys.* **59**, 725 (1986).
6. G. JOYCE AND M. LAMPE, *Phys. Fluids* **26**, 3377 (1983).
7. G. JOYCE AND M. LAMPE, *J. Comput. Phys.* **63**, 398 (1986).
8. M. LAMPE, W. M. SHARP, R. F. HUBBARD, E. P. LEE, AND R. H. BRIGGS, *Phys. Fluids* **27**, 2921 (1984).
9. E. P. LEE, F. W. CHAMBERS, L. L. LODESTRO, AND S. S. YU, in *Proceedings, of the 2nd Intl. Topical Conf. on High Power Electron Beam Research and Technology*, edited by J. A. Nation and R. N. Sudan (Cornell Uiv. Press, Ithaca, NY, 1977), Vol. I, p. 381.
10. R. L. FEINSTEIN, D. A. KEELEY, E. R. PARKINSON, AND W. REINSTRA, Science Applications International Corp. Report SAIC-U-74-PA-DOE, 1984 (unpublished).
11. W. S. SHARP, S. S. YU, AND E. P. LEE, Lawrence Livermore National Laboratory Report UCID-21114, 1987 (unpublished).
12. E. P. LEE, Lawrence Livermore National Laboratory Report UCID-17286, 1976 (unpublished).
13. B. HUI AND M. LAMPE, *J. Comput. Phys.* **55** 328 (1984).
14. D. S. HARNED AND W. KERNER, *J. Comput. Phys.* **60**, 162 (1985).
15. F. W. CHAMBERS, Lawrence Livermore National Laboratory Report UCID-18302, 1979 (unpublished).
16. T. P. HUGHES AND B. B. GODFREY, *Phys. Fluids.* **27**, 1531, (1984).
17. J. C. CLARK, K. W. STRUVE, S. S. YU, AND R. E. MELENDEZ, in *Proceedings, 5th Intl. Conf. on High-Power Particle Beams*, edited by R. J. Briggs and A. J. Toepfer (Lawrence Livermore National Laboratory, Livermore, 1983), p. 412.
18. W. M. SHARP, M. LAMPE, AND H. S. UHM, *Phys. Fluids* **25**, 1456 (1984).